RESEARCH ARTICLE

A Dual-sensitive Hydrogel Based on Poly(Lactide-co-Glycolide)-Polyethylene Glycol-Poly(Lactide-co-Glycolide) Block Copolymers for 3D Printing

Yang Zhou[1], Yuecheng Cui[1], Li-Qun Wang[1,2]*

[1]MOE Key Laboratory of Macromolecular Synthesis and Functionalization, Department of Polymer Science and Engineering, Zhejiang University, Hangzhou 310027, P. R. China
[2]Hangzhou Medsun Biological Technology Co., Ltd, Hangzhou Economic and Technological Development Area, Hangzhou 310027, P. R. China

Abstract: The thermo-sensitive hydrogel formed by triblock copolymers of polyethylene glycols and aliphatic polyesters serves as a promising candidate for bioink due to its excellent biodegradability and biocompatibility. However, the thermo-crosslinking alone cannot achieve a robust hydrogel to support the 3D printed constructs without collapse. Herein, a photo-crosslinkable group was introduced into the triblock copolymers to achieve a dual-sensitive hydrogel. A triblock copolymer poly(lactide-co-glycolide)-polyethylene glycol-poly(lactide-co-glycolide) decorated with acrylate group in the chain end was prepared. The obtained aqueous solutions of the copolymers could transform into hydrogels with excellent shear thinning properties and rapid elastic recovery properties spontaneously on the increase of temperature. The resulted thermogels also allowed for photo-crosslinking by exposure to ultraviolet radiation, with storage modulus dramatically increased to stable the printed constructs. Through a two-step crosslinking strategy, complicated tissue-like constructs with high shape fidelity can be printed using the dual-sensitive inks. Moreover, the mechanical strength, swelling ratio, and printability of the hydrogels can be tuned by varying the substitution rate of the acrylate group without compromising the inks' extrudability. We expect that the dual-sensitive hydrogels may be used as bioinks to print large constructs for applications in tissue engineering.

Keywords: 3D bioprinting; Dual-sensitive hydrogels; Poly(lactide-co-glycolide)-polyethylene glycol-poly(lactide-co-glycolide); Injectable hydrogels

*Correspondence to: Li-Qun Wang, Department of Polymer Science and Engineering, Zhejiang University, Hangzhou 310027, P. R. China; lqwang@zju.edu.cn

Received: April 29, 2021; **Accepted:** June 22, 2021; **Published online**: June 29, 2021

Citation: Zhou Y, Cui YC, Wang LQ, 2021, A Dual-sensitive Hydrogel Based on Poly(Lactide-Co-Glycolide)-Polyethylene Glycol-Poly(Lactide-Co-Glycolide) Block Copolymers for 3D Printing. *Int J Bioprint*, 7(3):389. http://doi.org/10.18063/ijb.v7i3.389

1. Introduction

Three-dimensional (3D) bioprinting is an emerging technology in the field of tissue engineering. The ability to rapidly create complicated biomimetic structures with high accuracy through layer-by-layer deposition make it a promising tool for patient-specific treatments[1-3]. Among several printing strategies, inkjet printing and laser-assisting bioprinting have high print resolutions but can only deal with nonviscous liquid[4,5]; stereolithography (STL) is fast but needs lots of ink to form a vat[6]; extrusion printing is the most widely used due to its easy implementation and ability to print large constructs[4,7]. Various biomaterials including synthetic and natural polymers have been reported as printing hydrogels, such as poly(ethylene glycol) (PEG)[3,8], collagen[9], gelatin[10], sodium alginate[11], silk fibroin[12-14], hyaluronic acid[15-17], and decellularized extracellular matrix[18]. Nevertheless, the number of compounds used as inks is still limited[6]. It is necessary to develop new inks to expand the inks library for further applications of 3D bioprinting.

© 2021 Zhou, *et al*. This is an Open Access article distributed under the terms of the Creative Commons Attribution License (https://creativecommons.org/licenses/by/4.0/), permitting distribution, and reproduction in any medium, provided the original work is properly cited.

Aqueous solutions of some ABA triblock copolymers, consisting of hydrophobic A and hydrophilic B blocks, will undergo a reversible sol-gel-sol transition with the increase of temperature[19-22]. One of the most commonly used copolymers is comprised of PEG as hydrophilic blocks and aliphatic polyester as the hydrophobic units. The polyester blocks can be poly(lactide-co-glycolide) (PLGA)[21,23], poly(caprolactone-co-lactide) [19,24], poly(caprolactone-co-glycolide) (PCGA) [25], polycaprolactone[20] and so on. At low temperatures, the triblock copolymers self-assemble into "flower-like" micelles and the solutions behave like liquid[26]. When the temperature is elevated, micelles aggregate to form a percolated network through hydrophobic interactions, resulting in a gel at the macroscopic level[22,27]. With many parameters such as block length of PEG and polyester[28], molecular weight distribution[21,23], end group[29], and even addition agent[28] can be used to adjust the sol-gel transition behavior. For their fast sol-gel transition between room and body temperature, these thermogels have been demonstrated potential applications as injectable hydrogels in drug delivery systems[30,31], tissue engineering[32,33], and prevention of post-operative adhesion[24].

We believe the thermal-sensitive copolymers hydrogel may serve as a promising candidate for bioink because of its excellent biodegradability and biocompatibility[34]. However, an ideal ink should fulfill certain rheological and mechanical requirements to achieve good extrudability as well as high shape fidelity. That is, it is required that the inks not only can be extruded easily as a smooth and uniform filament but also can maintain sufficient mechanical strength to support the printed structure without collapse[20,22]. Although the thermogels can be extruded as a fiber[35], their mechanical strength is still too weak to support large complicated objects. Therefore, it is desired to improve the mechanical strength of the hydrogel to meet the need of 3D printing.

At present, the introduction of new cross-linking mechanisms such as host-guest interaction[15,36,37], metal ions coordination[38], photopolymerization[10,39,40], chemical coupling reaction[41,42], and enzyme-catalyzed reaction[16,43,44] is the most common way to enhance the physical strength of inks. The thermo-sensitive physical hydrogel could also be strengthened through the formation of new crosslinks. For example, Ohya's group decorated the triblock copolymer PCGA-PEG-PCGA with succinimide ester groups at the termini and then crosslinked with polyamines. However, the modified copolymers were insoluble in water and a crosslinking agent was needed to form a covalent network. Most importantly, nearly no improvement on modulus was observed due to the low reaction efficacy[25]. Thus, it is desired to provide the thermogels with a more effective crosslinking to enhance their physical strength. The photopolymerization crosslinking system, which has been used to improve the printability of polymers such as gelatin[45], sodium alginate[46], silk fibroin[14], hyaluronic acid[15,17], and PEG[3,41,47], is a good choice due to its rapid solidification and controllable gelation by ultraviolet (UV) radiation.

In this study, the thermo-sensitive and photo-sensitive hydrogels based on triblock copolymers PLGA-PEG-PLGA were explored as inks. To obtain the dual-sensitive hydrogels, the copolymers were first synthesized by ring-opening polymerization, followed by esterification of the hydroxyl group with acrylic acid (**Figure S1**). The thermo-induced gelation was used to adjust the rheological properties of the hydrogels, yielding a printable ink that could hold its predesigned shapes during extrusion. Afterward, the printed scaffolds were fixed by UV photopolymerization crosslinking with the enhancement of physical strength. A variety of constructs, including a human nose, were successfully printed with high shape fidelity through the two-step crosslinking strategy. Moreover, by mixing with unmodified copolymers (**Figure 1A**), the mechanical properties, swelling ratio, and printability of inks could be easily tailored without compromising their extrudability. It is believed that this dual-sensitive hydrogel can be used as bioinks for printing large tissue-like constructs in the future.

2. Materials and methods

2.1. Materials

PEG with a number-average molecular weight of 1500 Da (PEG1500) was purchased from Sigma-Aldrich (St. Louis, USA). The monomers *L*-lactide and glycolide were gifted by Medsun (Hangzhou, China). *N,N'*-dicyclohexylcarbodiimide (DCC), 4-dimethylaminopyridine (DMAP), acrylic acid, and tin 2-ethylhexanoate [$Sn(Oct)_2$] were obtained from Aladdin (Shanghai, China). The photoinitiator, lithium phenyl-2,4,6-trimethylbenzoylphosphinate (LAP) was received from TCI (Tokyo, Japan). Anhydrous diethyl ether, methylene dichloride (DCM), and other chemicals were all chemical regent grade and bought from Shanghai Chemical Reagents Co. (Shanghai, China). PEG1500 was dehydrated before the experiments, and other reagents were all used as received.

2.2. Synthesis of the triblock copolymer

The triblock copolymers PLGA-PEG-PLGA were synthesized by ring-opening copolymerization of L-LA and GA in the presence of PEG1500 as an initiator and $Sn(Oct)_2$ as a catalyst (**Figure S1**). The detailed synthesis procedure of P1 was shown as following. Dehydrated PEG1500 (7.5 g, 5 mmol), *L*-LA (11.4027 g, 68.69 mmol), GA (9.1855 g, 68.69 mmol), and $Sn(Oct)_2$ (3 – 5 drops) were weighed and added to a 250-mL round-bottom flask.

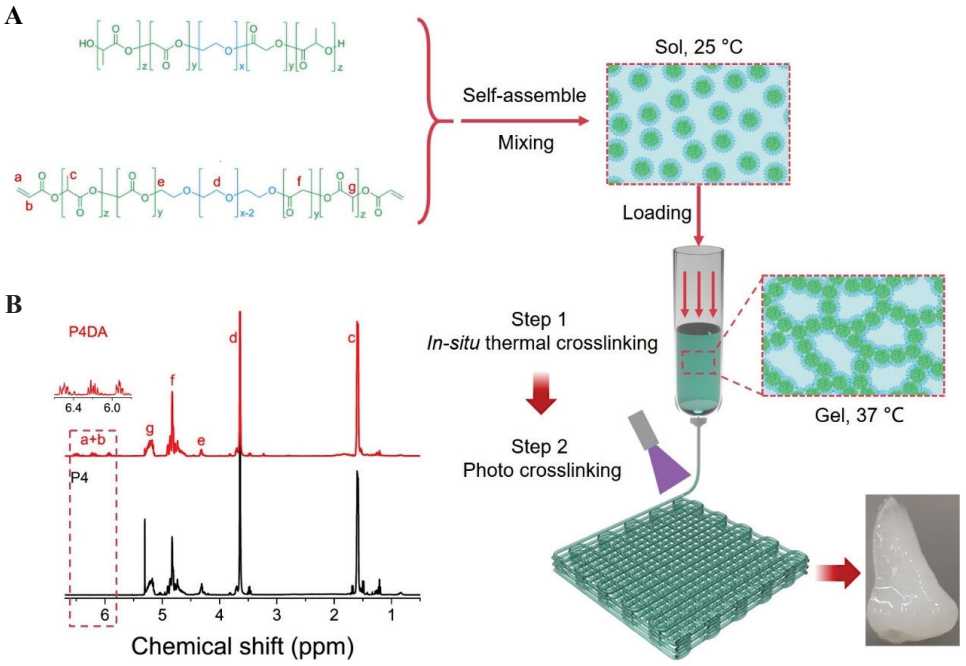

Figure 1. (A) Schematic of the 3D printing process through the dual-sensitive hydrogel inks. (B) ^{1}H-NMR spectra of P4 and P4DA.

Next, the flask was kept under reduced pressure at 60°C for 30 min to remove residual air and then filled with dry argon. With stirring, polymerization was carried out under argon protection at 160°C for 8 h. After cooling to room temperature, the crude product was dissolved in DCM (10 mL) and purified by reprecipitation using cold diethyl ether as a poor solvent. Then, the precipitate was dried in vacuo at r.t. for 3 days to yield the product. P2, P3, and P4 with different PLGA lengths were all acquired using similar procedures by varying the feed ratio.

P4DA was synthesized by esterification of P4 and acrylic acid as described in **Figure S1**. Firstly, P4 (21.08 g, 5 mmol) was dissolved in 30 mL DCM and transferred to a 250 mL flask. Then, DCC (3.095 g, 15 mmol) and DMAP (0.1832 g, 1.5 mmol) dissolved in 20 mL DCM were added to the flask and the solution was cooled to about 0°C in an ice-water bath under argon. At last, acrylic acid was added drop wise in 20 min through an addition funnel with a pressure-equalization arm. The reaction solution was stirred at 0°C for 2 h and further reacted at r.t. for 20 h. A small amount of water was added to stop the reaction and exhaust remained DCC. The reaction mixture was filtered by suction filtration to remove dicyclohexylurea. The filtrate was concentrated to 20 mL and precipitated 3 times using an excess of cold ethyl ether. After drying in vacuo for 3 days, the product was stored at −24°C.

2.3. Structural characterization

The ^{1}H-NMR spectra were recorded on an NMR spectrometer (Bruker, DMX-400MHz). $CDCl_3$ was used as deuterated solvent and the concentration of copolymer was 10 mg/mL. The number-average molecular weights of PLGA (M_n) can be calculated from ^{1}H-NMR spectra. The weight-average molecular weights (M_w) and polydispersity index (Đ) of copolymers were measured by GPC (TSK, D40). Tetrahydrofuran was used as mobile phase at a flow rate of 1.0 mL/min at 40°C and calibrated with polystyrene standards. The Fourier-transform infrared (FTIR) spectra of P4 and P4DA were scanned on an FTIR spectrometer (Thermo Scientific, Nicolet 6700) in the range of 4000-400 cm^{-1}. KBr pellets painted with samples were used for testing. The absorbance of P4 and P4DA was recorded on a UV spectrophotometer (Shimadzu, UV-1800) in the range of 200 – 400 nm. The copolymers were dissolved in water at a concentration of 0.05 wt.%.

2.4. Preparation of copolymer solutions

Unless otherwise specified, all the samples were prepared using deionized water here. To obtain copolymer solutions, a given volume of water was added to a vial with copolymer, followed by stirring with a magnetic stir bar below 30°C. The dissolution process lasted for 2 – 3 days until the polymer was completely dissolved and homogeneous solutions were achieved. For printing experiments, a series of solutions were prepared by blending P1 and P4DA. The total copolymer concentration was fixed at 25 wt.%, while the fraction of P4DA was varied. The prepared solutions were named DA00, DA20, DA40, DA60, and DA100, where the number referred to wt.% of P4DA in the total polymer. All the samples were

kept at 4°C before use. LAP was added as an initiator with a dosage of 0.003 wt.%.

2.5. Vial-inverting test

The sol-gel transition of the copolymer aqueous solutions was examined by the vial-inverting method. The vials containing 1 mL solution were immersed in a water bath. The temperature was adjusted from 25 to 55°C with an increment of 1°C/step. Samples were equilibrated for 10 min at each temperature and then the state was confirmed. If no flow was noticed in 20 s after the vial was inverted, the state of the solution was regarded as "gel," otherwise a "sol" state would be recorded.

2.6. Rheological analysis

(1) Sol-gel transition

A rotational rheometer (TA, DHR) was used to investigate the sol-gel-sol transition of the copolymer solutions and the properties of the hydrogel. Temperature sweep experiments were performed to examine the phase transition phenomenon using a cone-plate geometry (1.985°, 40 mm diameters, 0.05 mm gap). About 0.7 mL solution was added between two plates at 25°C. Then, the margin of the plate was covered with lowly viscous oil to prevent vaporization of the solvent. The temperature was increased from 25 to 55°C at a rate of 2°C/min. The controlled stress and frequency were 1.0 Pa and 6.28 rad/s, respectively.

(2) Extrudability

After adding to the plate, all the samples were then kept at 37°C for 5 min before measurement. To characterize the shear thinning nature of the hydrogel, the shear rate was logarithmically increased in a range of 0.1 – 100 s^{-1} and the viscosity was recorded. The elastic recovery behavior was measured by alternating 1% and 100% strain for 100 s at 6.28 rad/s angular frequency. The thixotropic property of the ink was proved using a three-stage steady-state flow test. At the first and the third stage, a shear rate of 0.1 s^{-1} was applied for 100 s. The shear rate was set to 100 s^{-1} and lasted for 5 s during the second stage.

(3) Mechanical properties

To compare the physical strength of hydrogels after photo-crosslinking, the samples were made into disks with 20 mm diameter and 1 mm thick by exposure to UV light (375 nm) for 300 s at 37°C. The disks were then tested on a parallel-plate (20 mm, 1.0 mm gap) fixture. A frequency sweep (1% strain, 0.1 – 50 rad/s angular frequency) was performed to examine the mechanical properties.

2.7. Tensile tests

A commercial tensile tester (Instron 3343) was used to measure tensile modulus of samples. After photo-crosslinked, the hydrogel was then cut into dumbbell-shaped specimens (gauge length, 12 mm; width, 2 mm; and thickness, 1 mm). All the experiments were conducted with a 50 N load cell and a stretch rate of 10 mm/min. At least three specimens were tested for each sample to get reliable data.

2.8. Swelling ratio

The water absorption properties were evaluated using the conventional gravimetric method. For this purpose, the inks were made into cylinder samples (4 mm height, 5 mm diameter) by exposure to UV light at 37°C for 5 min. The hydrogels were then immersed in 5 mL deionized water at 37°C for 48 h. After that, samples were taken out and the surface water was wiped carefully with filter papers, the swollen hydrogels were weighted and noted as W_s. Then, those samples were lyophilized and the dry weight (W_r) was recorded. Similar studies were conducted in triplicates, and the swelling ratio (s_r) was calculated using the equation.

$$s_r = \frac{W_s - W_d}{W_d} \times 100\%$$

2.9. Degradation properties

To study the degradation properties of the dual-sensitive hydrogel, 0.5 mL solution was added to a vial and then exposed to UV light for 5 min at 37°C. After gelation, 1 mL phosphate buffer saline (PBS) containing 0.02 mg lipase was added. The degradation experiments were conducted at 37°C and PBS was refreshed every day. At specific time intervals, the residual samples were taken out and freeze-dried. The weight was recorded and the weight loss to the original weight of samples before incubation was seen as the degradation rate. All the experiments were performed in triplicates and the average value was used for analysis.

2.10. Printing experiments

(1) Preparations before printing

The printing was performed in a commercial microextrusion 3D bioprinter (Regenovo, Bio-Architect®-Pro) with a temperature-controlled syringe and print bed. The control of the printer was achieved through software (Bio-Architect v2.2) on a personal computer. First, a printing model was designed in 3D computer-aided design and saved as STL files. Those files were imported to the software, and then the walking path was generated automatically according to the printing parameters. To print, inks were loaded into 10 mL syringes and store at 4°C for 2 h to remove bubbles. After those syringes were mounted onto the printing apparatus, equilibrating at 37°C for 15 min was required to make sure the inks stay at a

gel state. Blunt-tipped stainless-steel needles were used here to reduce the influence of environmental temperature. During the printing process, the temperature of the syringe and print bed was controlled at 37°C and an UV light lamp (UltraFire, 501 B) was applied to photo-crosslink the inks.

(2) Assessment of printability

To assess and compare the printability of inks, lattice structures ($20 \times 20 \times 0.5$ mm^3) were printed onto a glass plate. The printing speed was set at 10 mm/s here and the pressure was adjusted between 0.05 MPa and 0.55 MPa according to the situation. Various needle size (0.16, 0.21, 0.31, 0.41, and 0.51 mm) and line interval (0.8, 1.0, 1.2, 1.6 mm) were used to optimize the printing parameters. Images were captured by a digital microscope (Dino-lite, FC-OC1) immediately after the printing was completed. The line width and square area of grids were measured in ImageJ. Diffusion rate (D_r) was calculated according to previous research by He *et al*.[48]

$$D_r = \frac{A_t - A_e}{A_t} \times 100\%$$

where A_t is the theoretical area of a square and A_e is the experimentally measured area of the square.

(3) Printing of large constructs

Centimeter-scale structures cuboid ($20 \times 20 \times 4$ mm^3), pyramid ($20 \times 20 \times 10$ mm^3), and human nose ($28 \times 18 \times 10$ mm^3) were printed using DA40. We designed the models of cuboid and pyramid, and the human nose structure was retrieved from an open-source website (https://www.thingiverse.com/thing:306031) with a slight modification.

2.11. *In vitro* cell viability analysis

Human primary fibroblasts in cell culture medium with copolymers at 5 mg/mL were added to a 96-well plate at a cell density of 500 cells/well. Subsequently, the cells were incubated for 3 days at 37°C in the presence of 5% CO_2. To evaluate the cell viabilities, a cytotoxicity assay kit (KeyGEN BioTECH, China) was used to stain the cells. Briefly, the cell culture medium was removed and washed with PBS for 3 times. 1 mL PBS containing 0.5 μL calcein AM and 0.5 μL PI was added to the samples. The samples were then incubated for 45 min at room temperature. At last, a fluorescence microscope (Leica, Germany) was used to observe live/dead fibroblasts.

3. Results and discussion

3.1. Synthesis and structure characterization of the triblock copolymer

The triblock copolymers were synthesized through ring-opening polymerization of LA and GA using PEG1500 as an initiator. Here, four copolymers with different PLGA lengths, P1, P2, P3, and P4, were prepared and investigated. Their molecular weight and molecular weight distribution were characterized using ^{1}H NMR and GPC. Detailed data for the four copolymers are listed in **Table 1**. To obtain the dual-sensitive hydrogels, all the copolymers were then reacted with acrylic acid, while only P4 with a shorter PLGA length could result in a soluble polymer due to the end-group effect[29]. To verify the success of the acylation, the ^{1}H NMR spectrum of P4DA and its precursor was showed and compared (**Figure 1B**). Different from P4, three new peaks were observed between 5.8 and 6.6 ppm in the spectrum of P4DA, corresponding to the three protons of acryloyl. This observation indicated that the hydroxy end groups were replaced with acryloyl groups, and the degree of substitution was calculated to be 102%. This conclusion was also supported by emerging characteristic peaks related to acryloyl in IR and UV absorption spectrums (**Figure S2**).

3.2. Thermo-sensitive sol-gel transition of copolymer solutions

Initially, the vial-inverting test was used to examine the sol-gel behavior (**Figure 2A**), with the results displayed in **Figure 2B**. The phase transition diagram showed a gel window of "U" shape, representing a sol-gel-sol process. P1 showed a gelation temperature range from 33 to 46°C, and its critical gelation concentration (CGC) was around 16 wt.%. With the decrease of molecular weight, P2 and P3 got a narrower gel window and a higher CGC (**Table 1**) due to less hydrophobicity of the polyester block. Although P4 was quite hydrophilic and soluble even at high temperature and high concentration, P4DA underwent sol-gel-sol transition with a gel window located at 37 – 52°C. Their differences in the macroscopic gelation behavior are associated with the increased hydrophobicity induced by new end groups. To be a bioink, it is necessary for a hydrogel to possess a wider gel window and a lower CGC; so that P1 and P4DA were chosen for further studies.

The sol-gel transition behavior was also investigated with rheological measurements. Typical results of temperature sweeps for P1 and P4DA are shown in **Figure 2C**. Both the storage modulus (G') and loss modulus (G'') raised rapidly from low values to a peak around body temperature and then tended to decrease. There were two crossover points in curves of G' and G'', the first intersection implied a transition of sol-gel and the second one was believed to be a gel-sol transition. The temperatures at the two intersection points were remarked as T_{gel} and T_{sol}, respectively. T_{gel} and T_{sol} of P4DA were determined to be 38.8 and 49.2°C, which was in agreement with previous results (**Figure 2B**).

Whereas the results of P1 (34.5 and 38.0°C) shown obvious differences with those in the phase diagram (35 and 43°C). This situation was likely due to a continuous increase of system viscosity even G' was overtaken by G'' after 38.0°C.

The salting-out effect of the photoinitiator (LAP) on the sol-gel transition behavior of P1 and P4DA was also examined. As shown in **Figure S3**, T_{gel} and T_{sol} of the P4DA were found to be decreased once LAP was added to the solutions. In addition, G' and G'' of P4DA dropped sharply when the temperature was elevated above T_{sol}, indicating a gel-precipitation process instead of a gel-sol transition (**Figure S3B**). In contrast, the sol-gel transition behavior of P1 was much less affected by the salting-out effect than that of P4DA, and no gel-precipitation transition was observed (**Figure S3A**).

A mixing strategy was employed to prepare a series of samples with different P4DA content to evaluate the extent of photo-crosslinking on the printability of inks. For this purpose, six samples of DA00, DA20, DA40, DA60, DA80, and DA100 were prepared by blending P1 with P4DA, the number represented the fraction of P4DA in the total copolymer. All of those samples were then evaluated with rheological tests, and the calculated T_{gel} and T_{sol} are shown in **Figure 2E**. Both T_{gel} and T_{sol} were linearly increased with the fraction of P4DA, and

Table 1. Molecular characterization and gelation information of synthesized triblock copolymers

Samples	M_n [a]	LA/GA[a]	Đ[b]	CGC/wt %[c]	Gel window/°C[c]
P1	2102-1500-2102	1/0.97	1.27	16	35 – 43
P2	1790-1500-1790	1/1.00	1.33	22	39 – 41
P3	1495-1500-1495	1/1.00	1.23	32	-
P4	1345-1500-1345	1/0.97	1.23	-	-
P4DA	1627-1500-1627	1/0.99	1.25	22	42 – 48

[a]Number-average molecular weight (M_n) and the molar ratio of lactide/glycolide (LA/GA) were calculated from ^{1}H NMR spectroscopy. [b]Molar-mass dispersity (Đ) was measured via GPC. [c]Critical gelation concentration (CGC) was acquired from phase diagrams and the gel window showed a gelation temperature range at concentration of 25 wt.%

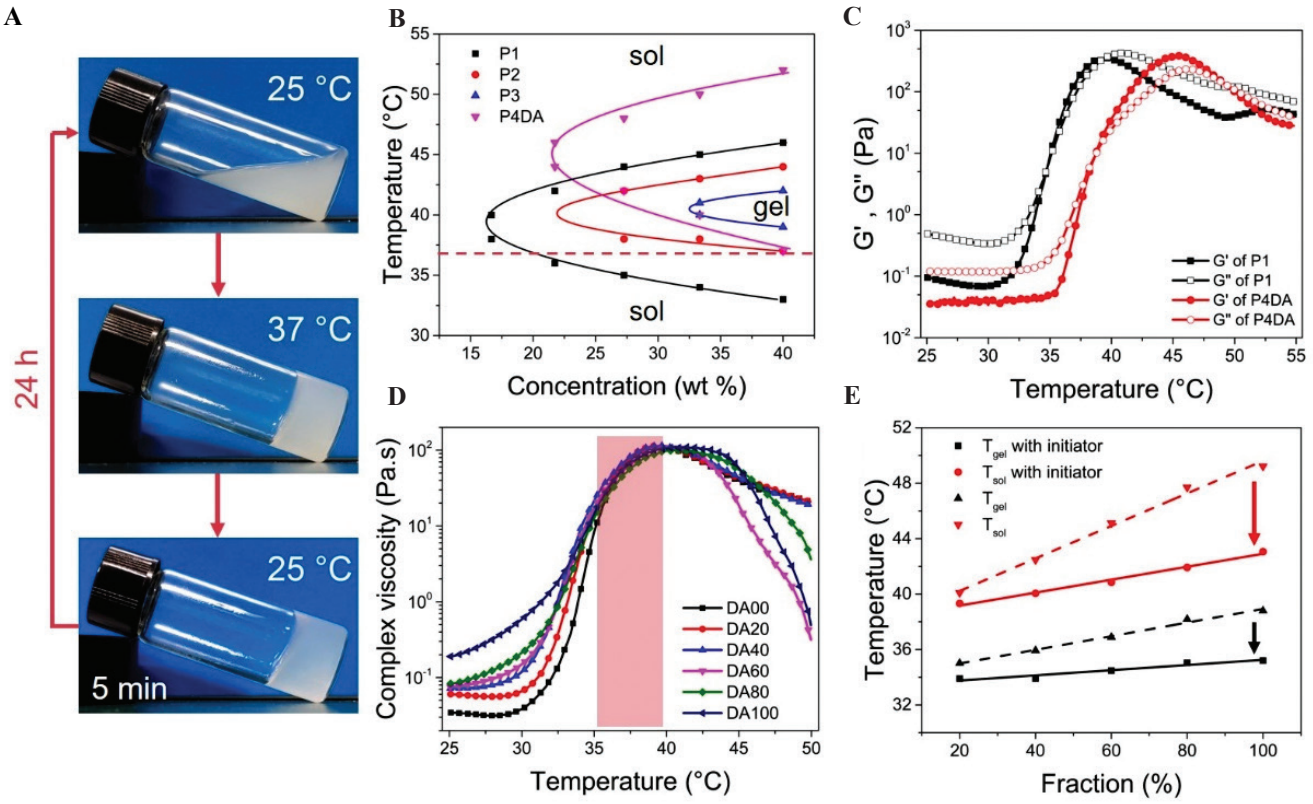

Figure 2. Thermo-sensitive sol-gel phase transition of samples. (A) Photographs of sample state at different temperature. (B) Phase diagrams of P1, P2, P3, and P4DA. (C) Storage modulus and loss modulus of P1 and P4DA as a function of temperature. (D) Complex viscosity of DA00, DA20, DA40, DA60, DA60, and DA100 with addition of photoinitiator as a function of temperature. (E) T_{gel} and T_{sol} of DA20, DA40, DA60, DA60, and DA100 with and without addition of photoinitiator.

so did the influence of salt-out effect on the transition temperature. More importantly, we found that all the samples showed similar curves in temperature sweeps (from 33 to 40°C) regardless of hydrogels composition (**Figure 3D**). The results indicated that the mechanical and other properties of the inks can be easily tuned by varying the fraction of P4DA without compromising its extrudability.

3.3. Assessment of extrudability

Through the temperature-induced sol-gel transition, the complex viscosity (above 10 Pa·s) of all the samples reached the requirement for a filament formation in the gelation temperature range from 35.2 to 39.1°C, **Figure 3D**[49]. To ascertain whether the thermogels were capable of printing, DA40 was loaded and extruded from a needle. As displayed in **Figure 3F**, filaments with a smooth and uniform morphology were extruded continuously from the printing nozzle when the printing temperature was set at 37°C. In contrast, only droplets were formed at the nozzle tip at 25°C. This result indicated that the extrudability of inks could be easily modulated by temperature. To achieve better printing results, all the printing experiments were conducted at 37°C.

The responsiveness of viscosity to shear rate was examined with rheological characterization. The flow curve of all samples demonstrated a linear decrease in viscosity with the increase of shear rate (**Figure 3A**), indicating their shear-thinning behavior. All the samples showed viscosity above 200 Pa·s at a shear rate of 0.01 s^{-1}, and it decreased to 0.05 Pa·s when the shear rate was increased to 100 s^{-1}.

Besides the shear-thinning properties, the rapid elastic recovery from disruption also contributed to high shape fidelity. Accordingly, elastic recovery tests were carried out using DA40 as a model with alternating low (1%) and high (100%) strain at 100 s intervals (**Figure 3B**). At a low strain of 1%, G' of hydrogel was greater than G'', implying a solid behavior, whereas a sharp drop was observed when the hydrogel was subjected to a high strain of 100%, and G' was surpassed by G''. After removal of applied high strain, G' of hydrogel instantly recovered to its initial value. The recovery of hydrogels remained unchanged after five cycles. Furthermore, a three-stage steady-flow test was set to simulate conditions before, during, and after the printing process (**Figure 3C**). At the first stage, the hydrogel showed a viscosity around 200 Pa·s with a low shear rate (0.1 s^{-1}) representing flow behavior in the barrel. A high shearing rate (100 s^{-1}) was followed to simulate the extrusion of inks, and the viscosity dropped sharply to 1 Pa·s at this stage. When high shearing force was removed as inks were extruded

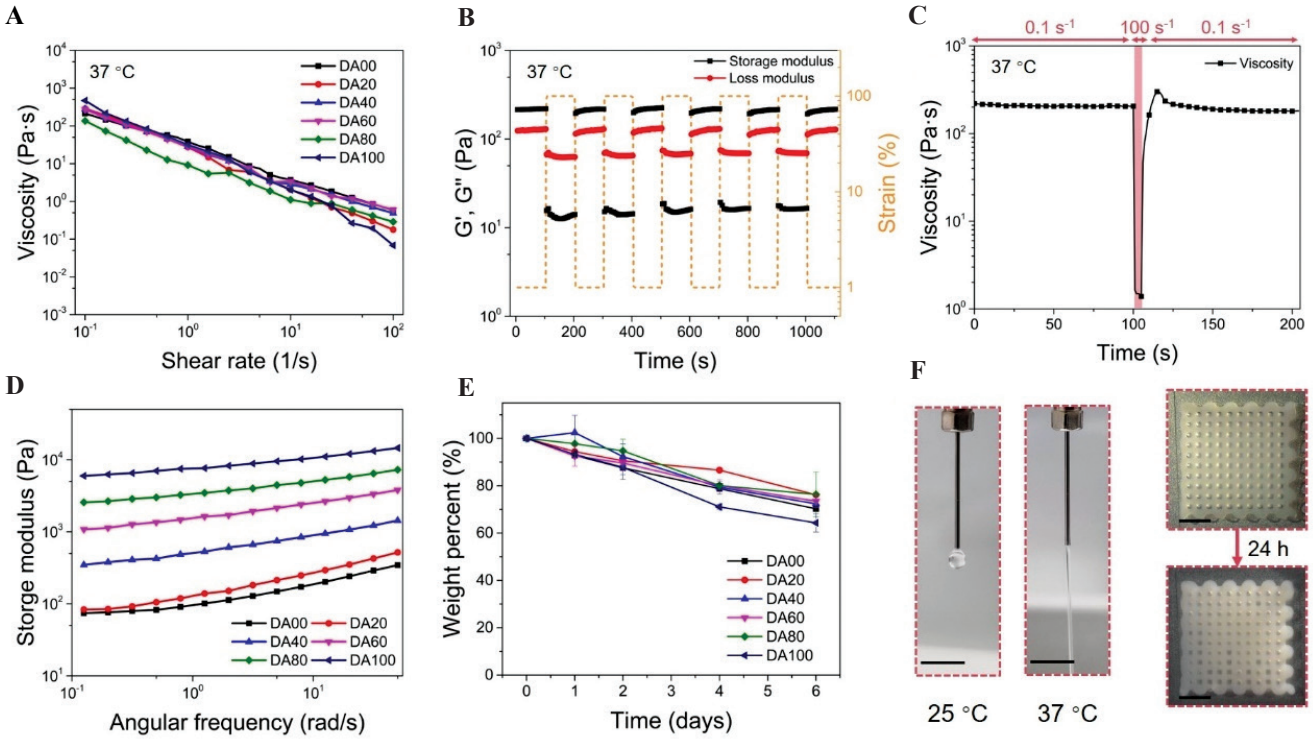

Figure 3. (A) Viscosity of DA00, DA20, DA40, DA60, DA60, and DA100 as a function of shear rate at 37°C. (B) Elastic recovery properties of DA40 at 37°C. (C) Shear recovery properties of DA40 at 37°C. (D) Storge modulus of DA00, DA20, DA40, DA60, DA60, and DA100 after photo-crosslinking as a function of frequency. (E) Degradation profiles of DA00, DA20, DA40, DA60, DA60, and DA100 at 37°C in PBS containing 0.02 mg lipase. (F) Effect of temperature on the filament formation of ink. (G) Photographs of printed construct with DA40 before and after immersing in water for 24 h (Scale bar: 5 mm).

out from the needle, viscosity bounced back to 180 Pa·s within 5 s, which was 90% recovery of its initial viscosity.

The above results suggested that the hydrogels possessed excellent shear-thinning and rapid recovery properties, which were mainly attributed to the reversible nature of physical bonding. Another worry on the thermo-sensitive inks was that the solid hydrogels would transform back into solutions at low environmental temperatures. But fortunately, the thermogels exhibited a slow de-gelling process; the viscosity of the system remained unchanged in 5 min even after the temperature was dropped from 37 to 25°C (**Figure 2A**). The self-supporting filament in the filament collapse experiments[50] also demonstrated that the inks could hold the printed constructs before the photo-crosslinking was constructed (**Figure 4G**).

3.4. Properties of the dual-sensitive hydrogel

Successful printing is dependent not only on the extrudability of inks but also on the ability to support the printed constructs. However, the thermo-sensitive hydrogel was a physical hydrogel with weak mechanical strength. The maximum value of G' in temperature sweep was only 500 Pa (**Figure 2C**), indicating poor shape retention of the hydrogels. To compare the mechanical strength of hydrogels after photo-crosslinking, G' of all samples was evaluated using frequency sweep tests. In **Figure 3D**, G' (at 1 rad/s) was increased from 90.7 Pa of DA00 to 7493.1 Pa of DA100, indicated that the mechanical strength was enhanced by the introduction of photo-crosslinking. Furthermore, this was also confirmed by the results of tensile tests, DA100 reached a tensile modulus of 21.9 kPa (**Figure S4**) but DA00 was too weak to form a specific shape for tests. In addition, the storage and tensile modulus tended to be higher when more P4DA was formulated into the inks. Therefore, by varying the fraction of P4DA in the inks, the hydrogels' mechanical strength can be tuned to satisfy a range of applications.

The swelling properties of the samples were investigated by immersing them in deionized water. DA00 (848.2%) and DA20 (844.26%) had a high swelling ratio because of the lack of effective covalent network formation. However, the swelling ratio of DA40 was decreased (771.7%), which was attributed to a denser hydrogel mesh formed by chemical crosslinking. As the fraction of P4DA further increased, the swelling ratio of DA60, DA80, and DA100 was decreased to 559.7%, 451.3%, and 430.0%, respectively. The higher swelling ratio of physical hydrogels was associated with low structural stability[51]. The reduced water absorption of dual-sensitive hydrogels vouched for good shape retention under cell culture over a long time (**Figure 3G**). The enzymatic degradation properties of the hydrogels were then evaluated. As displayed in **Figure 3E**, all the samples showed close degradation profiles regardless of the fraction of P4DA, implying that the excellent biodegradation properties of thermogels were not affected by the introduction of the covalent network.

3.5. Printing of the dual-sensitive hydrogel inks

To evaluate the printability of the dual-sensitive hydrogel inks, lattice structure was printed with DA00, DA20, DA40, DA60, DA80, and DA100. As shown in **Figure 4A**, multi-layer grids printed with DA00 and DA20 collapsed, square holes in the structure transformed into circular ones due to diffusion of filaments, showing their poor shape retention. In contrast, constructs with the well-defined structure were obtained in experiments of DA40, DA60, DA80, and DA100. And their diffusion rate, a parameter to evaluate ink's shape fidelity[48] was around 35%, much lower than that of DA00 (97.20%) and DA20 (78.80%). In addition, diameters of filament (line width) were used to quantitatively assess the printability of different inks. DA00 and DA20 showed an unacceptable line width (1.37 and 0.93 mm), which was three-fold larger than the needle diameters (0.31 mm). Nevertheless, the line width of DA40, DA60, DA80, and DA100 was, respectively, determined to be 0.44, 0.47, 0.46, and 0.53 mm, which was quite close to the diameters of needle. There was no doubt that the printability of the inks was improved by the addition of P4DA, which was attributed to enhanced mechanical strength due to the formation of covalent networks. Therefore, inks with P4DA fraction above 40 wt.% were expected to be used in further experiments.

Next, DA40 was chosen as a model to explore the influence of printing parameters on the inks' printability. The needles with different diameters were used to print the inks. The results showed that the inks could be extruded from all needles with diameters from 0.16 mm to 0.53 mm (**Figure 4B**). However, the smaller the diameters of the needle, the higher pressure was needed to extrude the inks. Besides, all the results showed a line width larger than their needle diameters (**Figure 4E**), which was attributed to the spreading of the weak thermo-sensitive hydrogel before photo-crosslinking. Filament interval, representing the distance a strand needed to span between filaments from the previous layer, is another important printing parament. As shown in the filament collapse study (**Figure 4G**), a sagging filament was observed between a large gap, which would result in poor shape fidelity. However, details of the printed constructs would disappear when a small interval was chosen due to diffusion of filament into the deep part of the construct (**Figure 4C and F**). For better printing results, a needle with 0.31 mm diameter and a filament interval of 1.2 mm was chosen for further experiments. With optimized parameters, a 10-layer lattice was printed and displayed in **Figure 4H**. The printed grid exhibited high shape fidelity; moreover, it could be held by hands, demonstrating the ink's ability to print large structures.

It is a challenge to print intricate 3D architectures of a soft hydrogel due to the lack of mechanical strength. To demonstrate the inks' ability to print centimeter-scale objects with high shape fidelity, a variety of constructs were printed. The printing was carried out using DA 40 with the optimized printing parameters. First, we printed a cuboid with the dimension of 20 × 20× 4 mm^3, the pictures in **Figure 5A** revealed high shape retention. And fusion of subsequent two layers was observed in the side view. Then, a more complicated pyramid (20 × 20 × 10 mm^3) was printed without collapsing (**Figure 5B**). At last, a self-supporting anatomical-size human nose (18 × 28 × 10 mm^3) was printed (**Figure 5C**). The printed construct showed high structural similarity to its 3D digital model in details, and no collapse was observed throughout the experiment.

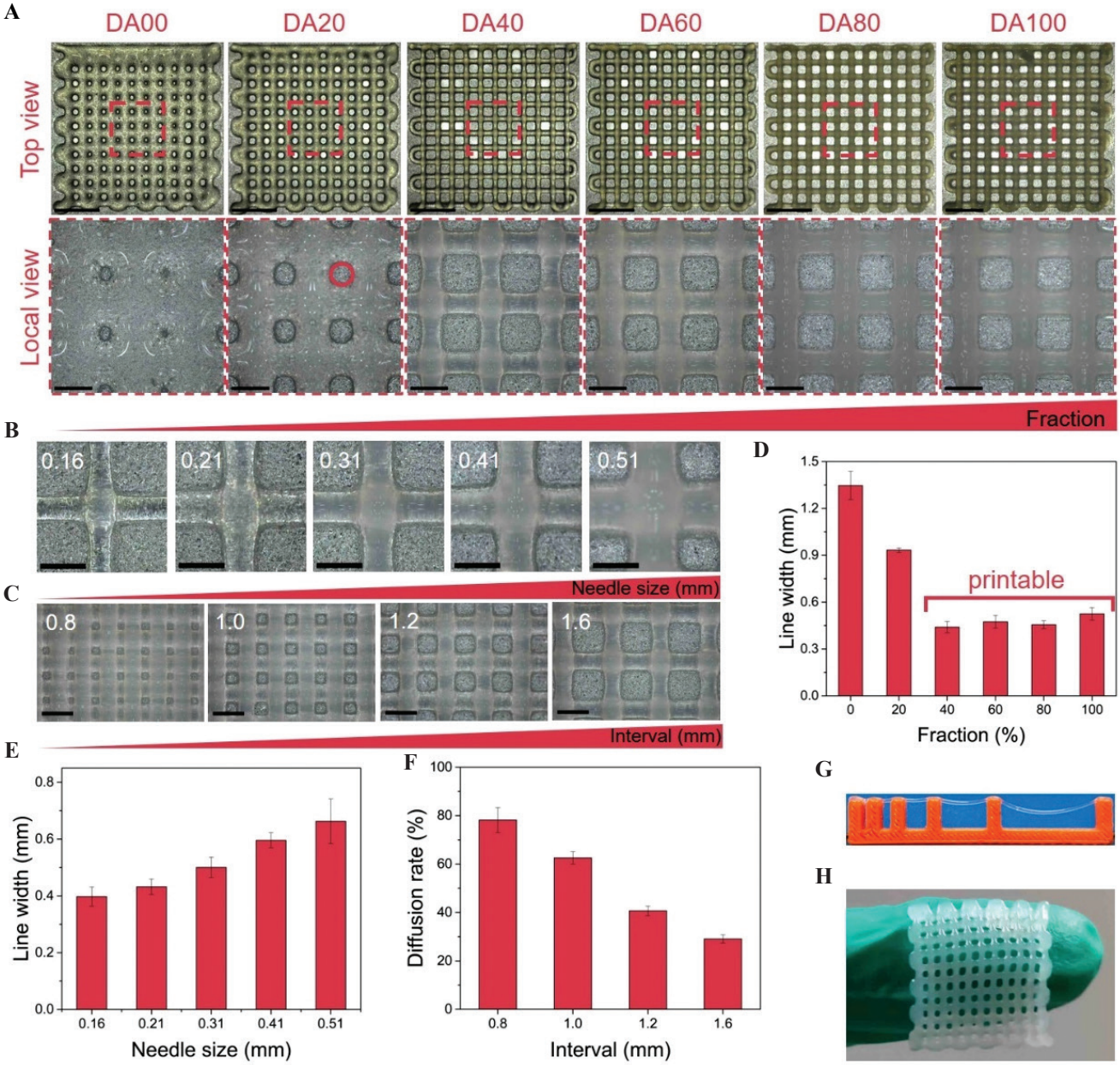

Figure 4. Printing of the dual-sensitive hydrogels inks. (A) Images of printed grids with DA00, DA20, DA40, DA60, DA60, and DA100 (scale bars in top view: 5 mm, in local view: 1 mm). Images of printed structures with DA40 using (B) different nozzle size and (C) different filament interval (scale bars: 1 mm). (D) Line width of DA00, DA20, DA40, DA60, DA60, and DA100 in printed lattices. (E) Line width of DA40 in printed lattices with different needle size. (F) Diffusion rate of DA40 in printed lattices with different filament interval. (G) Photograph of printed strand on a construct with pillars. (H) Photograph of a printed multi-layers construct moved by hands.

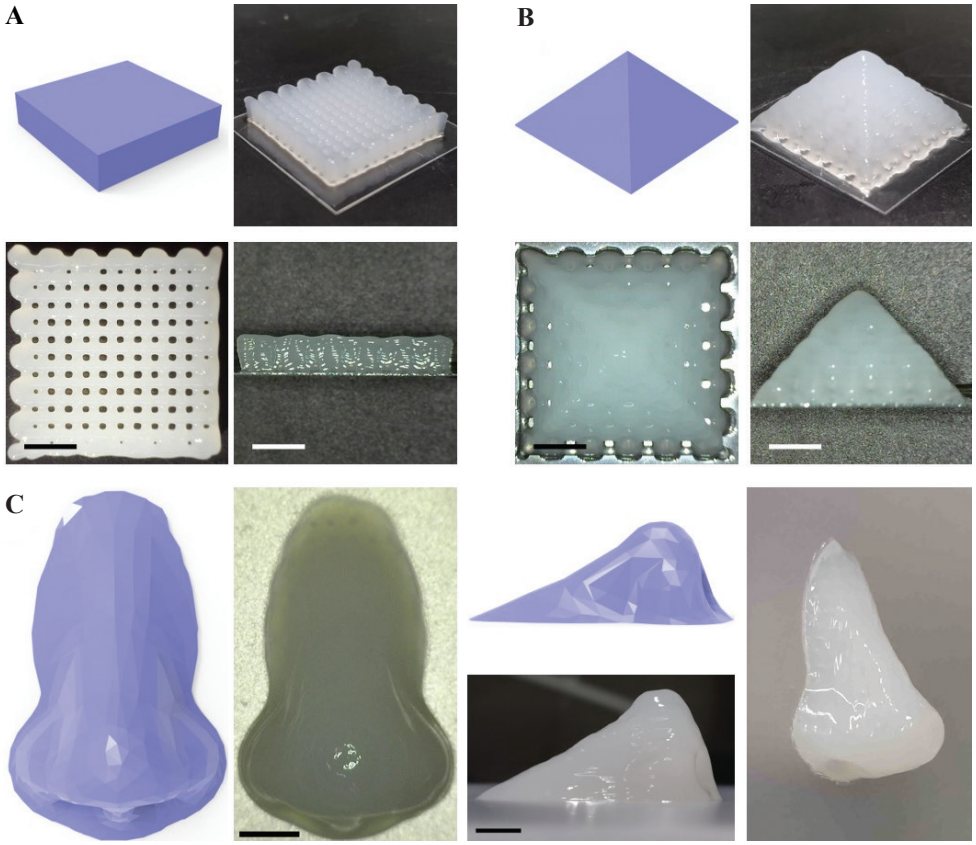

Figure 5. Images of printed constructs. (A) Cuboid (20 × 20 × 4 mm^3). (B) Pyramid (20 × 20 × 10 mm^3). (C) Human nose (28 × 18 × 10 mm^3). Scale bars: 5 mm.

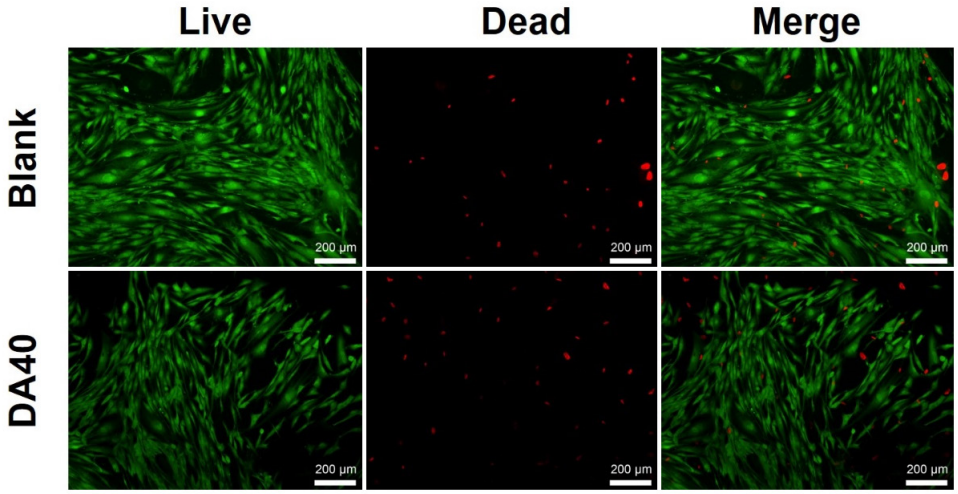

Figure 6. Fluorescent microscopic images of fibroblast cultured with DA40 (5 mg/mL) and with medium only.

3.6. *In vitro* cell viability analysis

Biocompatibility is also an important factor to evaluate a bioink; a cell viability test was performed using human primary fibroblasts to estimate the cell cytotoxicity of the copolymers. Live/dead staining was used to determine the cell viability over 3 days of culture. Fluorescence microscopy images (**Figure 6**) showed that 90% of cells were viable, which was similar to that in the blank control (92%). This result showed that the copolymers possess good cell compatibility, indicating that the inks may be printed to biodegradable scaffold for tissue engineering.

4. Conclusions

In summary, a thermo-sensitive and photo-sensitive hydrogel based on the triblock copolymers PLGA-PEG-PLGA was developed for 3D printing. Aqueous solutions of the copolymers exhibited thermo-induced sol-gel transition accompanied by the increase of the viscosity. The resulted hydrogels showed excellent shear-thinning properties and fast elastic recovery properties, which rendered the thermogels with good extrudability while maintaining the predesigned structures. Furthermore, the thermogels allowed for UV photopolymerization to stabilize the printed scaffolds, with storage modulus dramatically increased. Through a two-step crosslinking strategy, complicated constructs with high shape fidelity can be printed. Moreover, the self-supporting printed scaffolds could be picked up by hand. The synthesis process of the dual-sensitive hydrogels was simple and low-cost, meaning that large-scale production in industrial manufacture was possible. The dual-sensitive hydrogels were expected to be promising bioinks, development of cell-laden inks and their applications in tissue engineering will be explored in future studies.

Acknowledgments

This work was financially supported by the National Key Research and Development Program of China (2017YFC1103400).

Conflict of interest

All authors declare that they have no conflicts of interest.

Author contributions

Y. Z. designed the experiments. Y. Z. and Y. C. performed the experiments and analyzed the results. Y. Z. wrote the manuscript. L. W. supervised the work and revised the manuscript.

References

1. Noor N, Shapira A, Edri R, *et al.*, 2019, 3D Printing of Personalized Thick and Perfusable Cardiac Patches and Hearts. *Adv Sci*, 6:1900344. https://doi.org/10.1002/advs.201900344
2. Kang HW, Lee SJ, Ko IK, *et al.*, 2016, A 3D Bioprinting System to Produce Human-scale Tissue Constructs with Structural Integrity. *Nat Biotechnol*, 34:312–9. https://doi.org/10.1038/nbt.3413
3. Grigoryan B, Paulsen SJ, Corbett DC, *et al.*, 2019, Multivascular Networks and Functional Intravascular Topologies within Biocompatible Hydrogels. *Science*, 364:458–64.
4. Bedell ML, Navara AM, Du Y, *et al.*, 2020, Polymeric Systems for Bioprinting. *Chem Rev*, 120:10744–92.
5. Li X, Liu B, Pei B, *et al.*, 2020, Inkjet Bioprinting of Biomaterials. *Chem Rev*, 120:10793–833.
6. Valot L, Martinez J, Mehdi A, *et al.*, 2019, Chemical Insights Into Bioinks for 3D Printing. *Chem Soc Rev*, 48:4049–86. https://doi.org/10.1039/c7cs00718c
7. Murphy SV, Atala A, 2014, 3D Bioprinting of Tissues and Organs. *Nat Biotechnol*, 32:773–85. https://doi.org/10.1038/nbt.2958
8. Jin Y, Liu C, Chai W, *et al.*, 2017, Self-Supporting Nanoclay as Internal Scaffold Material for Direct Printing of Soft Hydrogel Composite Structures in Air. *ACS Appl Mater Interfaces*, 9:17456–65. https://doi.org/10.1021/acsami.7b03613
9. Lee A, Hudson AR, Shiwarski DJ, *et al.*, 2019, 3D Bioprinting of Collagen to Rebuild Components of the Human Heart. *Science*, 365:482–7.
10. Yin J, Yan M, Wang Y, *et al.*, 2018, 3D Bioprinting of Low-Concentration Cell-Laden Gelatin Methacrylate (GelMA) Bioinks with a Two-Step Cross-linking Strategy. *ACS Appl Mater Interfaces*, 10:6849–57. https://doi.org/10.1021/acsami.7b16059.s001
11. Colosi C, Shin SR, Manoharan V, *et al.*, 2016, Microfluidic Bioprinting of Heterogeneous 3D Tissue Constructs Using Low-Viscosity Bioink. *Adv Mater*, 28:677–84. https://doi.org/10.1002/adma.201503310
12. Singh YP, Bandyopadhyay A, Mandal BB, 2019, 3D Bioprinting Using Cross-Linker-Free Silk-Gelatin Bioink for Cartilage Tissue Engineering. *ACS Appl Mater Interfaces*, 11:33684–96. https://doi.org/10.1021/acsami.9b11644
13. Schacht K, Jungst T, Schweinlin M, *et al.*, 2015, Biofabrication of Cell-Loaded 3D Spider Silk Constructs. *Angew Chem Int Ed*, 54:2816–20. https://doi.org/10.1002/anie.201409846
14. Kim SH, Yeon YK, Lee JM, *et al.*, 2018, Precisely Printable and Biocompatible Silk Fibroin Bioink for Digital Light Processing 3D Printing. *Nat Commun*, 9:1620. https://doi.org/10.1038/s41467-018-04517-w
15. Highley CB, Rodell CB, Burdick JA, 2015, Direct 3D Printing of Shear-Thinning Hydrogels into Self-Healing Hydrogels. *Adv Mater*, 27:5075–9. https://doi.org/10.1002/adma.201501234
16. Petta D, Armiento A R, Grijpma D, *et al.*, 2018, 3D Bioprinting of a Hyaluronan Bioink through Enzymatic-and Visible Light-Crosslinking. *Biofabrication*, 10:044104.

https://doi.org/10.1088/1758-5090/aadf58

17. Shi L, Carstensen H, Hölzl K, *et al.*, 2017, Dynamic Coordination Chemistry Enables Free Directional Printing of Biopolymer Hydrogel. *Chem Mater*, 29:5816–23. https://doi.org/10.1021/acs.chemmater.7b00128.s001
18. Pati F, Jang J, Ha DH, *et al.*, 2014, Printing Three-Dimensional Tissue Analogues with Decellularized Extracellular Matrix Bioink. *Nat Commun*, 5:3935. https://doi.org/10.1038/ncomms4935
19. Nielsen JE, Zhu K, Sande SA, *et al.*, 2017, Structural and Rheological Properties of Temperature-Responsive Amphiphilic Triblock Copolymers in Aqueous Media. *J Phys Chem B*, 121:4885–99. https://doi.org/10.1021/acs.jpcb.7b01174.s001
20. Bae SJ, Suh JM, Sohn YS, *et al.*, 2005, Thermogelling Poly (Caprolactone-b-Ethylene Glycol-b-Caprolactone) Aqueous Solutions. *Macromolecules*, 38:5260–5. https://doi.org/10.1021/ma050489m
21. Chen L, Ci T, Li T, *et al.*, 2014, Effects of Molecular Weight Distribution of Amphiphilic Block Copolymers on Their Solubility, Micellization, and Temperature-Induced Sol-Gel Transition in Water. *Macromolecules*, 47:5895–903. https://doi.org/10.1021/ma501110p
22. Cui S, Yu L, Ding J, 2019, Thermogelling of Amphiphilic Block Copolymers in Water: ABA Type Versus AB or BAB Type. *Macromolecules*, 52:3697–715. https://doi.org/10.1021/acs.macromol.9b00534
23. Chen L, Ci T, Yu L, *et al.*, 2015, Effects of Molecular Weight and Its Distribution of PEG Block on Micellization and Thermogellability of PLGA-PEG-PLGA Copolymer Aqueous Solutions. *Macromolecules*, 48:3662–71. https://doi.org/10.1021/acs.macromol.5b00168
24. Zhang Z, Ni J, Chen L, *et al.*, 2011, Biodegradable and Thermoreversible PCLA-PEG-PCLA Hydrogel as a Barrier for Prevention of Post-Operative Adhesion. *Biomaterials*, 32:4725–36. https://doi.org/10.1016/j.biomaterials.2011.03.046
25. Yoshida Y, Kawahara K, Inamoto K, *et al.*, 2016, Biodegradable Injectable Polymer Systems Exhibiting Temperature-Responsive Irreversible Sol-to-Gel Transition by Covalent Bond Formation. *ACS Biomater Sci Eng*, 3:56–67. https://doi.org/10.1021/acsbiomaterials.6b00581.s001
26. Vidyasagar A, Ku SH, Kim M, *et al.*, 2017, Design and Characterization of a PVLA-PEG-PVLA Thermosensitive and Biodegradable Hydrogel. *ACS Macro Lett*, 6:1134–9. https://doi.org/10.1021/acsmacrolett.7b00523
27. Cui S, Yu L, Ding J, 2018, Semi-Bald Micelles and Corresponding Percolated Micelle Networks of Thermogels. *Macromolecules*, 51:6405–20. https://doi.org/10.1021/acs.macromol.8b01014
28. Jeong B, Bae YH, Kim SW, 1999, Thermoreversible Gelation of PEG-PLGA-PEG Triblock Copolymer Aqueous Solutions. *Macromolecules*, 32:7064–9. https://doi.org/10.1021/ma9908999
29. Yu L, Zhang H, Ding J, 2006, A Subtle End-Group Effect on Macroscopic Physical Gelation of Triblock Copolymer Aqueous Solutions. *Angew Chem Int Ed*, 45:2232–5. https://doi.org/10.1002/anie.200503575
30. Zhou X, He X, Shi K, *et al.*, 2020, Injectable Thermosensitive Hydrogel Containing Erlotinib-Loaded Hollow Mesoporous Silica Nanoparticles as a Localized Drug Delivery System for NSCLC Therapy. *Adv Sci*, 7:2001442. https://doi.org/10.1002/advs.202001442
31. Ci T, Shen Y, Cui S, *et al.*, 2017, Achieving High Drug Loading and Sustained Release of Hydrophobic Drugs in Hydrogels through *In Situ* Crystallization. *Macromol Biosci*, 17:1600299. https://doi.org/10.1002/mabi.201600299
32. Ni P, Ding Q, Fan M, *et al.*, 2014, Injectable Thermosensitive PEG-PCL-PEG Hydrogel/acellular Bone Matrix Composite for Bone Regeneration in Cranial Defects. *Biomaterials*, 35:236–48. https://doi.org/10.1016/j.biomaterials.2013.10.016
33. Zhang Z, Lai Y, Yu L, *et al.*, 2010, Effects of Immobilizing Sites of RGD Peptides in Amphiphilic Block Copolymers on Efficacy of Cell Adhesion. *Biomaterials*, 31:7873–82. https://doi.org/10.1016/j.biomaterials.2010.07.014
34. Yu L, Ding J, 2008, Injectable Hydrogels as Unique Biomedical Materials. *Chem Soc Rev*, 37:1473–81. https://doi.org/10.1039/b713009k
35. Park MH, Joo MK, Choi BG, *et al.*, 2012, Biodegradable Thermogels. *Acc Chem Res*, 45:424–33.
36. Song KH, Highley C B, Rouff A, *et al.*, 2018, Complex 3D-Printed Microchannels within Cell-Degradable Hydrogels. *Adv Funct Mater*, 28:1801331. https://doi.org/10.1002/adfm.201801331
37. Wang Z, An G, Zhu Y, *et al.*, 2019, 3D-Printable Self-Healing and Mechanically Reinforced Hydrogels with Host-Guest Non-Covalent Interactions Integrated Into Covalently Linked Networks. *Mater Horiz*, 6:733–42. https://doi.org/10.1039/c8mh01208c
38. Wlodarczyk-Biegun MK, Paez JI, Villiou M, *et al.*, 2020, Printability Study of Metal Ion Crosslinked PEG-Catechol Based Inks. *Biofabrication*, 12:035009. https://doi.org/10.1088/1758-5090/ab673a

39. Chimene D, Peak CW, Gentry JL, *et al.*, 2018, Nanoengineered Ionic-Covalent Entanglement (NICE) Bioinks for 3D Bioprinting. *ACS Appl Mater Interfaces*, 10:9957–68. https://doi.org/10.1021/acsami.7b19808
40. Pi Q, Maharjan S, Yan X, *et al.*, 2018, Digitally Tunable Microfluidic Bioprinting of Multilayered Cannular Tissues. *Adv Mater*, 30:1706913. https://doi.org/10.1002/adma.201706913
41. Rutz AL, Gargus ES, Hyland KE, *et al.*, 2019, Employing PEG Crosslinkers to Optimize Cell Viability in Gel Phase Bioinks and Tailor Post Printing Mechanical Properties. *Acta Biomater*, 99:121–32. https://doi.org/10.1016/j.actbio.2019.09.007
42. Rutz AL, Hyland KE, Jakus AE, *et al.*, 2015, A Multimaterial Bioink Method for 3D Printing Tunable, Cell-Compatible Hydrogels. *Adv Mater*, 27:1607–14. https://doi.org/10.1002/adma.201405076
43. Mehrotra S, de Melo BA, Hirano M, *et al.*, 2020, Nonmulberry Silk Based Ink for Fabricating Mechanically Robust Cardiac Patches and Endothelialized Myocardium-on-a-Chip Application. *Adv Funct Mater*, 30:1907436. https://doi.org/10.1002/adfm.201907436
44. Sakai S, Mochizuki K, Qu Y, *et al.*, 2018, Peroxidase-Catalyzed Microextrusion Bioprinting of Cell-laden Hydrogel Constructs in Vaporized ppm-Level Hydrogen Peroxide. *Biofabrication*, 10:045007. https://doi.org/10.1088/1758-5090/aadc9e
45. Yue K, Trujillo-de Santiago G, Alvarez MM, *et al.*, 2015, Synthesis, Properties, and Biomedical Applications of Gelatin Methacryloyl (GelMA) Hydrogels. *Biomaterials*, 73:254–71. https://doi.org/10.1016/j.biomaterials.2015.08.045
46. Kirillova A, Maxson R, Stoychev G, *et al.*, 2017, 4D Biofabrication Using Shape-Morphing Hydrogels. *Adv Mater*, 29:1703443. https://doi.org/10.1002/adma.201703443
47. Peak CW, Stein J, Gold KA, *et al.*, 2018, Nanoengineered Colloidal Inks for 3D Bioprinting. *Langmuir*, 34:917–25. https://doi.org/10.1021/acs.langmuir.7b02540
48. He Y, Yang F, Zhao H, *et al.*, 2016, Research on the Printability of Hydrogels in 3D Bioprinting. *Sci Rep*, 6:29977.
49. Ouyang L, Yao R, Zhao Y, *et al.*, 2016, Effect of Bioink Properties on Printability and Cell Viability for 3D Bioplotting of Embryonic Stem Cells. *Biofabrication*, 8:035020. https://doi.org/10.1088/1758-5090/8/3/035020
50. Ribeiro A, Blokzijl MM, Levato R, *et al.*, 2017, Assessing Bioink Shape Fidelity to Aid Material Development in 3D Bioprinting. *Biofabrication*, 10:014102. https://doi.org/10.1088/1758-5090/aa90e2
51. Xu C, Lee W, Dai G, *et al.*, 2018, Highly Elastic Biodegradable Single-Network Hydrogel for Cell Printing. *ACS Appl Mater Interfaces*, 10:9969–79. https://doi.org/10.1021/acsami.8b01294